SIAM J. APPL. MATH.
Vol. 59, No. 2, pp. 700–724

ASYMPTOTIC AND COMPUTATIONAL ANALYSIS OF LARGE SHEAR DEFORMATIONS OF A THERMOPLASTIC MATERIAL*

D. A. EDWARDS† AND D. A. FRENCH‡

Abstract. Asymptotic results are presented for a simplified model for shear-band formation which neglects the effects of diffusion but still captures much of the important dynamics. Regular perturbation expansions fail, so a uniform expansion is constructed which tracks the divergent behavior of the simplified model. Severe computational difficulties exist in the form of finite-time blowup of the temperature and strain rate for the simplified model, but an adaptive numerical scheme tracks the severe blowup behavior well. This method, which is second-order accurate and has automatic mesh- and time-step refinement capabilities, also captures the severe band narrowing and strain rate growth in solutions to the full model with heat conduction. Comparison between the asymptotic and numerical methods shows good agreement, and remarks are made regarding asymptotic solutions of the full model.

Key words. adaptivity, asymptotics, finite differences, shear bands, singular perturbations, thermoplastic materials

AMS subject classifications. 35B25, 35C20, 65M05, 73E50

PII. S0036139997322419

1. Introduction.

Shear bands are thin regions of high strain that develop in materials under intense thermoplastic shear deformations. Since they often lead to premature failure in the material, it is important for scientists to understand them. They are observed in many physical processes, including armor penetration and high-speed machining. Study of the solution behavior is difficult due to the rapid growth of temperature, strain, and strain rate within the band as well as the severe localization or narrowing of the band itself. See Figures 6.6–6.9 for a sample of the severe behavior experienced in this problem. The book by Bai and Dodd [1] gives a background discussion of the area as well as many references.

Shear bands are of such interest that many researchers, using different techniques, have attempted to study them. Batra [2] and Batra and Ko [3] have studied shear-band formation using adaptive numerical methods in one and two dimensions. Bayliss et al. [4] have performed a numerical study with a highly accurate spectral method. DiLellio and Olmstead [7], [8] considered asymptotic solutions of shear bands when the velocity of the material is considered to be a known discontinuous function across the shear band. Drew and Flaherty [9] did a numerical study of a similar shear band model, using an adaptive moving-grid scheme. Maddocks and Malek-Madani [15] have analyzed the steady-state equations and found a Liapunov functional in the case of a particular constitutive stress-strain relationship. Needleman studied the shear band problem in [16]. Tzavaras [19] has given several rigorous analyses of shear-band

*Received by the editors June 9, 1997; accepted for publication (in revised form) February 27, 1998; published electronically December 2, 1998.
http://www.siam.org/journals/siap/59-2/32241.html

†Department of Mathematics, University of Maryland at College Park, College Park, MD 20742-4015. Current address: Department of Mathematical Sciences, University of Delaware, Newark, DE 19716-2553 (edwards@math.udel.edu). The research of this author was supported by National Science Foundation grant DMS-9407531.

‡Department of Mathematical Sciences, University of Cincinnati, Cincinnati, OH 45221-0025 (donald.french@uc.edu). This author was a visitor at the Department of Mathematics, University of Maryland at Baltimore County, Baltimore, MD, during most of the course of this work. The research of this author was partially supported by a grant from the Taft Foundation.

models. Wright and Walter [24] performed several numerical studies of the shear-band model (also see [24] for more papers by Wright on modeling and asymptotics, as well as [20], [22], and [23]). Finally, we note the recent numerical work by Glimm, Plohr, and Sharp [12], [13].

In section 2, we provide a systematic derivation of the mathematical model for this process, which involves a system of partial differential equations. By making several reasonable assumptions, we are able to simplify our model. In sections 3 and 4, we construct a regular perturbation expansion that tracks the true solution until blowup begins. The regular perturbation expansion is found to be flawed, and in section 5, a uniform perturbation approximation is derived that tracks the blowup behavior more accurately. Using a second-order, implicit finite-difference method with automatic mesh- and time-step refinement, described in section 6, we also find numerical approximations for the solutions. These numerical results demonstrate good qualitative agreement with our analytical solutions. We then include the effects of heat conduction and note that the resulting system cannot support unbounded solutions. However, numerical solutions exhibit severe band narrowing and extreme growth in strain rate, and hence our adaptive scheme is well-suited to capture the physical behavior. Last, we make some remarks in section 7 regarding the asymptotic solution of the more robust model.

2. Governing equations. We begin with the dimensional equations governing our model. First, we have the balance of linear momentum, neglecting pressure and gravitational forces:

$$\rho \frac{D\tilde{\mathbf{v}}}{D\tilde{t}} = \nabla \cdot \tilde{\tau}, \tag{2.1}$$

where ρ is the density, $\tilde{\mathbf{v}}$ is the velocity, $\tilde{t}$ is time, and $\tilde{\tau}$ is the stress tensor. In (2.1) we treat ρ as a constant. Also, we have the dimensional energy balance:

$$\rho C_p \frac{D\tilde{\theta}}{D\tilde{t}} = k\nabla^2\tilde{\theta} + \tilde{\tau} : \dot{\tilde{\Gamma}}_p, \tag{2.2}$$

where C_p is the heat capacity at constant pressure, $\tilde{\theta}$ is the temperature, k is the thermal conductivity, and $\dot{\tilde{\Gamma}}_p$ is the rate of plastic strain tensor. The second term on the right-hand side models the conversion of plastic work into thermal energy. The plastic strain rate is given by the following stress-strain relation:

$$\frac{\partial\tilde{\tau}}{\partial\tilde{t}} = \mathcal{C}\left(\nabla\tilde{\mathbf{v}} - \dot{\tilde{\Gamma}}_p\right), \tag{2.3}$$

where $\mathcal{C}$ is the constitutive 4-tensor of elastic moduli.

We wish to model a solid on the interval $-H \le \tilde{x} \le H$ undergoing a simple shearing motion in the $\tilde{y}$ direction. Therefore, the only velocity in the problem is $\tilde{v}_{\tilde{y}}$ and the only variations are in $\tilde{x}$, so (2.1)–(2.3) become

$$\rho \frac{\partial\tilde{v}_{\tilde{y}}}{\partial\tilde{t}} = \frac{\partial\tilde{\tau}_{\tilde{x}\tilde{y}}}{\partial\tilde{x}}, \tag{2.4}$$

$$\rho C_p \frac{\partial\tilde{\theta}}{\partial\tilde{t}} = k\frac{\partial^2\tilde{\theta}}{\partial\tilde{x}^2} + \tilde{\tau}_{\tilde{x}\tilde{y}}\dot{\tilde{\Gamma}}_{\tilde{x}\tilde{y},p}, \tag{2.5}$$

$$\frac{\partial \tilde{\tau}_{\tilde{x}\tilde{y}}}{\partial \tilde{t}} = \mu \left(\frac{\partial \tilde{v}_{\tilde{y}}}{\partial \tilde{x}} - \dot{\tilde{\Gamma}}_{\tilde{x}\tilde{y},p} \right), \tag{2.6}$$

where μ is the elastic shear modulus. In addition, we need a constitutive relation that connects $\tilde{\tau}_{\tilde{x}\tilde{y}}$ to the other parameters in the problem:

$$\tilde{\tau}_{\tilde{x}\tilde{y}} \left(\tilde{\theta}, \dot{\tilde{\Gamma}}_{\tilde{x}\tilde{y},p} \right) = \frac{\kappa}{\tilde{g}'(\tilde{\theta})} \dot{\tilde{\Gamma}}^{m}_{\tilde{x}\tilde{y},p}, \tag{2.7}$$

where m is a constant, κ is the stress-hardening coefficient, and $\tilde{g}'(\tilde{\theta})$ models the dependence of the stress on temperature. Here the prime indicates differentiation with respect to the argument—we have introduced the prime into $\tilde{g}$ to simplify things later on.

It is often the case in applications that m is quite small for many metals; however, in this paper we will not use it for a perturbation parameter. We expect the stress to decrease as the temperature gets large (see the introduction in Wright [22]), and so we require that

$$\lim_{\tilde{\theta} \to \infty} \tilde{g}'(\tilde{\theta}) = \infty. \tag{2.8}$$

An equation of the form of (2.7) (without the temperature dependence) is called an *Ostwald-de Waele* model [5] in fluid dynamics.

We postulate an arbitrary initial temperature distribution:

$$\tilde{\theta}(\tilde{x}, 0) = \tilde{\theta}_i(\tilde{x}). \tag{2.9}$$

We assume that the ends are insulated:

$$\frac{\partial \tilde{\theta}}{\partial \tilde{x}}(-H, \tilde{t}) = 0, \quad \frac{\partial \tilde{\theta}}{\partial \tilde{x}}(H, \tilde{t}) = 0. \tag{2.10}$$

The simple shear is modeled by a velocity given initially and at the boundaries:

$$\tilde{v}_{\tilde{y}}(\tilde{x}, 0) = \tilde{v}_i \frac{\tilde{x}}{H}, \quad \tilde{v}_{\tilde{y}}(-H, \tilde{t}) = -\tilde{v}_i, \quad \tilde{v}_{\tilde{y}}(H, \tilde{t}) = \tilde{v}_i. \tag{2.11}$$

Motivated by [24], we introduce dimensionless variables as follows:

$$\tilde{x} = Hx, \quad \tilde{\theta}(\tilde{x}, \tilde{t}) = \theta_c \theta(x, t), \quad \tilde{v}_{\tilde{y}}(\tilde{x}, \tilde{t}) = H\dot{\gamma}_c v(x, t), \quad \tilde{g}'(\tilde{\theta}) = \dot{\gamma}_c^m g'(\theta), \tag{2.12}$$

$$\tilde{t} = \frac{t}{\dot{\gamma}_c}, \quad \tilde{\tau}_{\tilde{x}\tilde{y}}(\tilde{x}, \tilde{t}) = \kappa\sigma(x, t), \quad \dot{\tilde{\Gamma}}_{\tilde{x}\tilde{y},\mathrm{p}}(\tilde{x}, \tilde{t}) = \dot{\gamma}_c \dot{\gamma}_p(x, t), \tag{2.13}$$

where θ_c is a characteristic temperature derived from the initial condition and $\dot{\gamma}_c$ is a characteristic strain rate for the problem. Introducing (2.12) and (2.13) into (2.6) yields

$$\frac{\kappa}{\mu} \frac{\partial \sigma}{\partial t} = \frac{\partial v}{\partial x} - \dot{\gamma}_p. \tag{2.14}$$

However, using our values for our parameters from the appendix, we see that $\kappa/\mu = 6.25 \times 10^{-3}$. Therefore, it is reasonable to make the simplifying assumption that $\kappa/\mu = 0$, which results in the *rigid/plastic approximation*. This assumption, which is

used in Glimm, Plohr, and Sharp [12], means that the stress evolution occurs on a much slower time scale than the others in the problem.

With this assumption, one can replace $\dot{\gamma}_p$ by $\partial v/\partial x$. Using this fact, (2.12), and (2.13) in (2.4), (2.5), and (2.7), we have

$$\frac{\partial v}{\partial t} = \alpha_1 \frac{\partial \sigma}{\partial x}, \tag{2.15}$$

$$\frac{\partial \theta}{\partial t} = \lambda \frac{\partial^2 \theta}{\partial x^2} + \alpha_2 \sigma \frac{\partial v}{\partial x}, \tag{2.16}$$

$$\sigma(x,t) = \frac{1}{g'(\theta)} \left(\frac{\partial v}{\partial x} \right)^m, \tag{2.17}$$

where

$$\alpha_1 = \frac{\kappa}{\rho H^2 \dot{\gamma}_c^2}, \qquad \alpha_2 = \frac{\kappa}{\rho C_p \theta_i}, \qquad \lambda = \frac{k}{\rho C_p H^2 \dot{\gamma}_c}, \tag{2.18}$$

and we have defined $g'(1) \equiv 1$.

Introducing our dimensionless variables into (2.9)–(2.11), we have new dimensionless boundary conditions:

$$\theta(x,0) = \theta_i(x), \tag{2.19}$$

$$\frac{\partial \theta}{\partial x}(1,t) = 0, \tag{2.20}$$

$$\frac{\partial \theta}{\partial x}(-1,t) = 0, \tag{2.21}$$

$$v(x,0) = v_i x, \tag{2.22}$$

$$v(1,t) = v_i, \tag{2.23}$$

$$v(-1,t) = -v_i. \tag{2.24}$$

We now make the simplifying assumption that $\theta_i(x)$ is even in x. In this case, we see from (2.15)–(2.24) that v is odd in x and θ is even in x. Therefore, we may redefine our problem on the interval $0 \le x \le 1$ with the following boundary conditions replacing (2.21) and (2.24):

$$\frac{\partial \theta}{\partial x}(0,t) = 0, \tag{2.25}$$

$$v(0,t) = 0. \tag{2.26}$$

3. The outer solution. The system (2.15)–(2.17), (2.19), (2.20), (2.22), (2.23), (2.25), and (2.26) is quite complicated to solve, even asymptotically. However, using our parameters from the appendix, we see that λ varies between 10^{-5} and 10^{-3}. Therefore, motivated by the analysis in [23], at first glance it may seem reasonable to set $\lambda = 0$ in (2.16), which corresponds to the total absence of diffusion. The resulting equation is

$$\frac{\partial \theta}{\partial t} = \alpha_2 \sigma \frac{\partial v}{\partial x}. \tag{3.1}$$

This substitution may be justified if any perturbation in the initial condition evolves on a length scale longer than the $O(\lambda^{1/2})$ scale associated with heat conduction. If this is true, then the magnitude of the heat conduction term in (2.16) will always be smaller than the other terms in the equation. Unfortunately, the phenomenon of shear-band formation involves the narrowing of the band over time (until the unloading stage, when it actually widens slightly; see section 6). Hence, as will be shown in the numerical simulations, structures often form which have length scales smaller than $O(\lambda^{1/2})$. Though this simplified model should thus be considered as a test of our asymptotic and numerical techniques, we shall examine the results to see if they qualitatively approximate the true physical system.

Some remarks on including diffusion in the asymptotics are presented in section 7, but for now we analyze the system with (3.1) replacing (2.16). We shall examine the resulting solutions to see how closely these asymptotic results model the full physical system. The results in this paper and their subsequent interpretation will then provide a useful foundation on which to base further examinations of extensions of the simplified model presented here.

We wish to examine the case where a small spatial discontinuity in the initial temperature distribution causes a shear band. Therefore, we define

$$\theta_i(x) = 1 + \epsilon f'(x/\epsilon), \quad f''(0) = 0, \quad 0 < \epsilon \ll 1. \tag{3.2}$$

The second condition in (3.2) follows from (2.25).

We begin by solving our problem in the "outer" region, that is, far from $x = 0$. We expand our functions in ϵ and neglect any transcendentally small terms. For reasons that will become clear later, we let

$$v(x,t) = v_0(x,t) + \epsilon^2 v_2(x,t) + o(\epsilon^2), \quad \theta(x,t) = z(x,t) + \epsilon^2 \theta_2(x,t) + o(\epsilon^2), \tag{3.3}$$

$$\sigma(x,t) = \sigma_0(x,t) + \epsilon^2 \sigma_2(x,t) + o(\epsilon^2). \tag{3.4}$$

Substituting (3.3) and (3.4) into (2.15), (3.1), and (2.17), we have, to leading orders,

$$\frac{\partial v_0}{\partial t} + \epsilon^2 \frac{\partial v_2}{\partial t} = \alpha_1 \left(\frac{\partial \sigma_0}{\partial x} + \epsilon^2 \frac{\partial \sigma_2}{\partial x} \right), \tag{3.5}$$

$$\frac{\partial z}{\partial t} + \epsilon^2 \frac{\partial \theta_2}{\partial t} = \alpha_2 \sigma_0 \frac{\partial v_0}{\partial x} + \alpha_2 \epsilon^2 \left(\sigma_2 \frac{\partial v_0}{\partial x} + \sigma_0 \frac{\partial v_2}{\partial x} \right), \tag{3.6}$$

$$\sigma_0 + \epsilon^2 \sigma_2 = \frac{1}{g'(z)} \left(\frac{\partial v_0}{\partial x} \right)^m + \epsilon^2 \sigma_0 \left[m \frac{\partial v_2}{\partial x} \left(\frac{\partial v_0}{\partial x} \right)^{-1} - \frac{g''(z)\theta_2}{g'(z)} \right]. \tag{3.7}$$

In addition, we have the following boundary conditions for our leading-order terms, which result from (3.2), (2.22), (2.26), and (2.23):

$$z(x,0) = 1, \tag{3.8}$$

$$v_0(x,0) = v_i x, \tag{3.9}$$

$$v_0(0,t) = 0, \quad v_0(1,t) = v_i. \tag{3.10}$$

We once again note that the initial condition (3.9) satisfies the boundary conditions (3.10) for all time, so we have

$$v_0(x,t) = v_i x. \tag{3.11}$$

Substituting (3.11) into (3.7) and (3.5), we have

$$\sigma_0 = \frac{v_i^m}{g'(z)}, \tag{3.12}$$

$$\frac{\partial \sigma_0}{\partial x} = 0. \tag{3.13}$$

Substituting (3.12) into (3.13), we may immediately conclude that $g'(z)$ (and hence z) is independent of x. Thus, we see that z immediately satisfies the no-flux boundary conditions (2.20) and (2.25). We then substitute (3.12) into (3.6) to obtain

$$\frac{dz}{dt} = \alpha_2 v_i \sigma_0, \tag{3.14}$$

$$g'(z)\frac{dz}{dt} = \alpha_2 v_i^{m+1}, \tag{3.15}$$

$$g(z) - g(1) = \alpha_2 v_i^{m+1} t, \tag{3.16}$$

where we have used (3.8).

We may invert (3.16) for any given $g(z)$ to find z. In particular, in order to compare with our numerics, we shall study the following expression:

$$g'(\theta) = \theta^p, \quad p > 0. \tag{3.17}$$

Note that this function satisfies our criterion that $g'(1) = 1$. Substituting (3.17) into (3.16) and inverting, we have

$$z(t) = (1 + \beta t)^{1/(p+1)}, \quad \beta = (p+1)\alpha_2 v_i^{m+1}. \tag{3.18}$$

We note that since our perturbation does not affect the outer solution, (3.18) is the solution to *all* orders unless an effect from the inner expansion perturbs the boundary conditions at $x = 0$.

4. The inner solution. To solve near $x = 0$, we transform to boundary-layer variables by letting

$$\xi = \frac{x}{\epsilon}, \quad \theta(x,t) = \hat{\theta}(\xi,t), \quad v(x,t) = \hat{v}(\xi,t), \quad \sigma(x,t) = \hat{\sigma}(\xi,t). \tag{4.1}$$

Doing so, (2.15), (3.1), (2.17), (3.2), (2.25), (2.22), and (2.26) become

$$\frac{\partial \hat{v}}{\partial t} = \frac{\alpha_1}{\epsilon}\frac{\partial \hat{\sigma}}{\partial \xi}, \tag{4.2}$$

$$\frac{\partial \hat{\theta}}{\partial t} = \frac{\alpha_2}{\epsilon}\hat{\sigma}\frac{\partial \hat{v}}{\partial \xi}, \tag{4.3}$$

$$\hat{\sigma} = \frac{1}{g'(\hat{\theta})\epsilon^m}\left(\frac{\partial \hat{v}}{\partial \xi}\right)^m, \tag{4.4}$$

$$\hat{\theta}(\xi,0) = 1 + \epsilon f'(\xi), \tag{4.5}$$

$$\frac{\partial \hat{\theta}}{\partial \xi}(0,t) = 0, \tag{4.6}$$

$$\hat{v}(\xi,0) = v_i\epsilon\xi, \tag{4.7}$$

$$\hat{v}(0,t) = 0. \tag{4.8}$$

To construct the proper expansions for our dependent variables, we note that to $O(1)$ the outer solution z satisfies all the necessary boundary and initial conditions, and hence we would not expect any $O(1)$ variation in $\hat{\theta}$. In addition, from our previous work we expect the velocity v to be undisturbed up to $O(\epsilon)$. Therefore, we let

$$\hat{v}(\xi,t) = v_i\epsilon\xi + \epsilon^2\hat{v}_2(\xi,t) + o(\epsilon^2), \quad \hat{\theta}(\xi,t) = z(t) + \epsilon\hat{\theta}_1(\xi,t) + o(\epsilon). \tag{4.9}$$

From (4.2), we see that we should let

$$\hat{\sigma}(\xi,t) = \sigma_0(t) + \epsilon\hat{\sigma}_1(\xi,t) + o(\epsilon). \tag{4.10}$$

Substituting (4.9) and (4.10) into (4.2)–(4.8), we have, to leading orders,

$$\epsilon^2\frac{\partial \hat{v}_2}{\partial t} = \alpha_1\frac{\partial \hat{\sigma}_1}{\partial \xi}, \tag{4.11}$$

$$\epsilon\frac{\partial \hat{\theta}_1}{\partial t} = \epsilon\left(\alpha_2\sigma_0\frac{\partial \hat{v}_2}{\partial \xi} + \alpha_2 v_i\hat{\sigma}_1\right), \tag{4.12}$$

$$\epsilon\hat{\sigma}_1 = \epsilon\frac{v_i^m}{g'(z)}\left[\frac{m}{v_i}\frac{\partial \hat{v}_2}{\partial \xi} - \frac{\hat{\theta}_1 g''(z)}{g'(z)}\right], \tag{4.13}$$

$$\hat{\theta}_1(\xi,0) = f'(\xi), \tag{4.14}$$

$$\frac{\partial \hat{\theta}_1}{\partial \xi}(0,t) = 0, \tag{4.15}$$

$$\hat{v}_2(\xi,0) = 0, \tag{4.16}$$

$$\hat{v}_2(0,t) = 0, \tag{4.17}$$

where we have used (3.12) and (3.14).

Substituting (4.13) into (4.11), we have

$$\frac{m}{v_i}\frac{\partial \hat{v}_2}{\partial \xi} - \frac{\hat{\theta}_1 g''(z)}{g'(z)} = \hat{\sigma}_1(t) = 0. \tag{4.18}$$

The last equality in (4.18) requires an explanation. We note that our $O(\epsilon)$ disturbance in θ decays as we reach the outer solution. Therefore, we expect no disturbance in the outer solution for the temperature to this order. In addition, our velocity profile also matches our outer solution to $O(\epsilon)$, so the only disturbance will be at $O(\epsilon^2)$. Therefore, we conclude that our solution given by (3.12) is good to $O(\epsilon^2)$, and hence (4.18) follows.

However, (4.18) cannot be satisfied by the initial conditions given by (4.14) and (4.16). Therefore, we must construct an initial layer in which $\hat{v}_2$ increases to satisfy (4.18). We need a layer in v_2, not in z, so we let

$$\eta = \frac{t}{\epsilon^2}, \quad \hat{\theta}(\xi,t) = 1 + \epsilon\Theta(\xi,\eta), \quad \hat{v}(x,t) = \epsilon v_i \xi + \epsilon^2 V(\xi,\eta), \tag{4.19}$$

$$\hat{\sigma}(x,t) \sim \Sigma(\xi,\eta). \tag{4.20}$$

Making these substitutions in (4.2), (4.3), and (2.17), we obtain

$$\epsilon\frac{\partial V}{\partial \eta} = \alpha_1 \frac{\partial \Sigma}{\partial \xi}, \tag{4.21}$$

$$\epsilon^{-1}\frac{\partial \Theta}{\partial \eta} = \alpha_2 \Sigma\left(v_i + \epsilon\frac{\partial V}{\partial \xi}\right), \tag{4.22}$$

$$\Sigma = v_i^m + \epsilon v_i^m\left[\frac{m}{v_i}\frac{\partial V}{\partial \xi} - \Theta g''(1)\right], \tag{4.23}$$

where we have used the fact that $g'(1) = 1$. In addition, (4.5)–(4.8) become

$$\Theta(\xi,0) = f'(\xi), \tag{4.24}$$

$$\frac{\partial \Theta}{\partial \xi}(0,\eta) = 0, \tag{4.25}$$

$$V(\xi,0)=0, \tag{4.26}$$

$$V(0,\eta)=0. \tag{4.27}$$

From (4.22), we see that we need an initial layer in V only, as expected. Therefore, we may use (4.24) as our expression for Θ throughout the region, and (4.21) becomes the following:

$$\frac{\partial V}{\partial \eta}=\alpha_1 v_i^m \frac{\partial}{\partial \xi}\left[\frac{m}{v_i}\frac{\partial V}{\partial \xi}-g''(1)f'(\xi)\right]. \tag{4.28}$$

Letting

$$h(\xi,\eta)=V(\xi,\eta)-\frac{v_i g''(1)f(\xi)}{m}, \tag{4.29}$$

we have

$$\frac{\partial h}{\partial \eta}=D\frac{\partial^2 h}{\partial \xi^2}, \quad D=\alpha_1 m v_i^{m-1}, \tag{4.30}$$

$$h(0,\eta)=0, \quad h(x,0)=-\frac{v_i g''(1)f(\xi)}{m}. \tag{4.31}$$

Equations (4.30) and (4.31) are easily solved using a Green's function approach [6, p. 26]; the solution for V is found to be

$$\begin{aligned} V(\xi,\eta)&=\frac{v_i g''(1)}{m}\\ &\times\left[f(\xi)-\frac{1}{2\sqrt{D\pi\eta}}\int_0^\infty f(\phi)\left\{\exp\left[-\frac{(\xi-\phi)^2}{4D\eta}\right]-\exp\left[-\frac{(\xi+\phi)^2}{4D\eta}\right]\right\}d\phi\right]. \end{aligned} \tag{4.32}$$

Since V as $\eta\to\infty$ must match to $\hat{v}_2$ as $t\to 0$, we have the following:

$$\hat{v}_2(\xi,0)=\frac{v_i g''(1)f(\xi)}{m}, \quad f(0)=0, \tag{4.33}$$

where the second condition comes from satisfying (4.27). Therefore, we see that in this initial layer the velocity adjusts itself so that (4.33) replaces (4.16). Note that (4.33) indeed solves (4.18) evaluated at $t=0$, as the initial condition should.

Using our expression for $\hat{\sigma}_1$ in (4.12), we may solve to obtain

$$\hat{\theta}_1(\xi,t)=f'(\xi)[g'(z)]^{1/m}, \tag{4.34}$$

where we have used (3.14), (4.14), and the fact that $g'(1)=1$. Note from (2.8) that our perturbation may grow without bound. The unbounded growth results from neglecting diffusion in our system, since physically we would expect heat to conduct away from the hot spot at the center of the band. Mathematically, we expect that as the temperature grows, its second spatial derivative would become so large that, even with the small coefficient λ, that term would balance the others in (2.16).

In addition, it will be shown in section 5 that our spatially dependent perturbation will eventually grow faster than our spatially homogeneous solution. This dominance

of the supposedly smaller first-order term, which occurs even in the presence of diffusion (as will be shown in section 7), is consistent with the idea of the formation of a shear band.

For completeness, we note that the uniformly valid solution is given by the inner solution

$$\theta(x,t) = z(t) + \epsilon f'(x/\epsilon)[g'(z)]^{1/m}. \tag{4.35}$$

Substituting (4.34) into (4.18), we have

$$\hat{v}_2(\xi,t) = \frac{v_i f(\xi)}{m}[g'(z)]^{1/m-1}g''(z), \tag{4.36}$$

where we have used (4.17). Therefore, a uniformly valid solution for the velocity is given by adding (4.36) and (4.32) and subtracting the common part, namely (4.33):

$$\begin{aligned} v(x,t) = v_i x + \epsilon^2 \frac{v_i}{m} \Bigg\{ & f(x/\epsilon)[g'(z)]^{1/m-1}g''(z) \\ & - \frac{g''(1)}{2\sqrt{D\pi t}} \int_0^\infty f(\phi/\epsilon) \left\{ \exp\left[-\frac{(x-\phi)^2}{4Dt}\right] - \exp\left[-\frac{(x+\phi)^2}{4Dt}\right] \right\} d\phi \Bigg\}. \end{aligned} \tag{4.37}$$

Once again, we note that this expression is good only to $O(\epsilon)$, since we have not calculated the necessary second-order term in the outer region.

For purposes of comparison with numerical results, we shall use $g'(\theta)$ as given in (3.17). In addition, we shall use a perturbation given by

$$f'(\xi) = e^{-\xi^2} \quad \Longrightarrow \quad f(\xi) = \frac{\sqrt{\pi}}{2} \operatorname{erf} \xi. \tag{4.38}$$

Using (4.38) and (3.17), we see that (4.35) becomes

$$\theta(x,t) = z + \epsilon e^{-(x/\epsilon)^2} z^{p/m}, \tag{4.39}$$

where z is given by (3.18). With our choice of $f(\xi)$ in (4.38), (4.37) becomes the following:

$$v(x,t) = v_i x + \epsilon^2 \frac{p v_i \sqrt{\pi}}{2m} \left[\operatorname{erf}(x/\epsilon) z^{p/m-1} - \operatorname{erf}\left(\frac{x}{\sqrt{4Dt+\epsilon^2}} \right) \right], \tag{4.40}$$

where z is once again given by (3.18) and we have used the fact that $g''(1) = p$.

Note that (4.40) does not satisfy (2.23) to $O(\epsilon^2)$. Therefore, a further expansion in the outer region would need to be constructed in order to satisfy (2.23) to higher accuracy.

5. Finite perturbations and blowup. From (4.39) we note that the second term in our perturbation solution grows without bound. In general, m is small, which means that we would expect this term to grow *faster* than our leading-order term. This growth in the narrow boundary layer is reminiscent of shear-band dynamics. However, this behavior violates the implicit assumption of the perturbation expansion: further terms in the expansion should always be smaller than the ones that come before.

We verify this by looking at the particular case given by (3.18) and (4.38). Checking (4.39) at $x = 0$, we see that the two terms are of the same size when

$$t = O\left(\epsilon^{m(p+1)/(m-p)}\right). \tag{5.1}$$

This bound on t is not very large because m is small.

Since we have seen that the $O(\epsilon)$ perturbation eventually causes an $O(1)$ effect, we now treat it as a finite perturbation by letting

$$\delta = \epsilon f'(\xi). \tag{5.2}$$

(The variable δ is used to remind us that this substitution does indeed represent something small.) This substitution is possible since ξ is basically a parameter in the analysis in section 4. This makes any derivative with respect to ξ on the order of ϵ. Though our velocity profile $\hat{v}$ does not depend in a straightforward way on δ, the derivative does, and hence we define the following new variables:

$$\hat{\theta}(\xi,t) = \hat{\theta}_0(\delta,t) + o(1), \quad \frac{\partial \hat{v}}{\partial \xi} = \epsilon w(\delta,t) + o(1). \tag{5.3}$$

Since $\partial v/\partial x = O(\epsilon)$, we see that $\hat{v} = O(\epsilon)$. Therefore, substituting (5.2) and (5.3) into (4.2), we have that $\partial \hat{\sigma}/\partial \delta = O(\epsilon)$.

Substituting (5.2) and (5.3) into (4.3)–(4.5) and (4.7) and expanding to leading orders, we have

$$\frac{\partial \hat{\theta}_0}{\partial t} = \alpha_2 w \hat{\sigma}, \tag{5.4}$$

$$\hat{\sigma} = \frac{w^m}{g'(\hat{\theta}_0)}, \tag{5.5}$$

$$\hat{\theta}_0(\delta,0) = 1 + \delta, \tag{5.6}$$

$$w(\delta,0) = v_i. \tag{5.7}$$

We note that (4.6) is satisfied by our definition of δ.

Since we know from our previous discussion that $\hat{\sigma}$ is a function of t only, we obtain

$$w = \frac{v_i g_m'(z)}{g_m'(\hat{\theta}_0)}, \tag{5.8}$$

where we have used (3.12). Substituting (5.8) into (5.4) and expanding to leading order, we have the following:

$$\frac{\partial \hat{\theta}_0}{\partial t} = \alpha_2 \sigma_0 \frac{v_i [g'(\hat{\theta}_0)]^{1/m}}{[g'(z)]^{1/m}}, \tag{5.9}$$

$$g_m'(\hat{\theta}_0)\frac{\partial \hat{\theta}_0}{\partial z} = g_m'(z), \tag{5.10}$$

where we have used (3.14).

Since $0 \le g_m'(z) \le 1$, we see that $g_m(z)$ must be strictly increasing. In addition, we note that

$$g_m'(\infty) = 0, \quad g_m'(1) = 1. \tag{5.11}$$

Lastly, we choose

$$g_m(\infty) = 0. \tag{5.12}$$

This is reasonable given (5.11), and any arbitrary constant can be taken out of the problem as shown below. Therefore, we see that $g_m(z) \leq 0$. Continuing to simplify, we obtain

$$\hat{\theta}_0 = g_m^{-1}\left(g_m(z) - g_m(1) + g_m(1+\delta)\right), \quad g_m^{-1}(g_m(z)) = z, \tag{5.13}$$

where we have used (3.8) and (5.6).

Equation (5.13) provides us with another form of our solution. Indeed, upon substituting $\delta = \epsilon f'(\xi)$ and expanding for small ϵ, one may verify that (5.13) does indeed replicate our results from section 4 to leading two orders. However, our expression (5.13) can also blow up, since $g_m^{-1}(0) = \infty$. Therefore, we must check the following equation:

$$g_m(z) = g_m(1) - g_m(1+\delta). \tag{5.14}$$

But (5.14) will always be satisfied. Why? Since g_m is strictly increasing, $g_m(1) < g_m(1) - g_m(1+\delta) < 0$. But $g_m(z)$ increases from $g_m(1)$ to zero as z goes from 1 to ∞. Therefore, (5.14) describes a monotonic curve $\delta_b = \delta(z)$ along which our solution blows up. As the solution diverges and our model breaks down, we see that we should include other effects into our model, such as the neglected plasticity and diffusion effects. We shall perform numerical calculations of the system where (2.16) replaces (3.1) in section 6; some remarks on asymptotic results are given in section 7.

In our special case given by (3.17) and (4.38), we have

$$\hat{\theta}_0 = \left\{ z^{1-p/m} - 1 + [1 + \epsilon e^{-(x/\epsilon)^2}]^{1-p/m} \right\}^{m/(m-p)}, \tag{5.15}$$

$$\frac{\partial v}{\partial x} = \frac{v_i}{z^{p/m}} \left\{ z^{1-p/m} - 1 + [1 + \epsilon e^{-(x/\epsilon)^2}]^{1-p/m} \right\}^{p/(m-p)}, \tag{5.16}$$

where z is again given by (3.18). In section 6 we shall compare the solutions given by (5.15), (5.16), (4.39), and (4.40) to those obtained by numerical results.

6. Numerical results. In this section we describe the results of our computations of the system of equations formulated in section 2, given by (2.15)–(2.19), (2.22), (2.23), and (2.25) with $g'(\theta) = \theta^2$, $v_i = 1$, $\theta_i(x) = 1 + \epsilon \exp(-(x/\epsilon)^2)$, and $\alpha_2 = 1$. We note that we will numerically solve the system with (2.16), not (3.1). However, for detailed comparisons with the asymptotics we shall set $\lambda = 0$.

For the computations, we use a finite-difference method that is a modification of the one described in [10]. The spatial and temporal derivatives are all approximated by centered differences, so we obtain second-order accuracy. Since the method is implicit, we use a fixed-point iteration to solve the system of nonlinear equations that arise at each time step. Automatic mesh refinement is implemented in the code to handle the narrowing of the shear band and the extreme behavior of the strain rate and temperature.

The numerical method consists of two nonlinear equations which are discretizations of (2.15) and (2.16) for the nth time step from t_n to t_{n+1} of width Δt. Velocity and temperature are the unknowns; the stress is eliminated using a discrete version

of (2.17). We discretize the nonlinear term in (2.17) using the following nonlinear difference:

$$\frac{1}{g'(\theta(\cdot,t+\Delta t/2))} \cong \frac{U(\theta(\cdot,t+\Delta t))-U(\theta(\cdot,t))}{\theta(\cdot,t+\Delta t)-\theta(\cdot,t)}, \tag{6.1}$$

where

$$U(\theta)=\int_0^\theta \frac{d\phi}{g'(\phi)}. \tag{6.2}$$

This form is motivated by the fact that for a similar system exhibiting blowup in finite time, French [10] has proven that such a discretization leads to numerical solutions that mimic the blowup of the true solution.

An iteration scheme is needed to solve the nonlinear equations for the velocity and temperature on time level t_{n+1}. We use the following extrapolations to linearize the nonlinear equations:

$$v^E(\cdot,t_{n+1}) = v(\cdot,t_n) + \Delta t\left[\frac{v(\cdot,t_n)-v(\cdot,t_{n-1})}{\Delta t}\right], \tag{6.3}$$

$$\theta^E(\cdot,t_{n+1}) = \theta(\cdot,t_n) + \Delta t\left[\frac{\theta(\cdot,t_n)-\theta(\cdot,t_{n-1})}{\Delta t}\right]. \tag{6.4}$$

The momentum balance equation (2.15) with the extrapolations, before applying the centered-difference discretization, has the form

$$\frac{\partial v}{\partial t} = \alpha_1 \frac{\partial}{\partial x}\left[\frac{1}{g'(\theta^E)}\left(\left|\frac{\partial v^E}{\partial x}\right|+d\right)^{m-1}\frac{\partial v}{\partial x}\right]. \tag{6.5}$$

The constant d is the unit roundoff and is used to regularize the factor $|\partial v/\partial x|^{m-1}$ in regions where v is nearly constant. The regularization in (6.5) is similar to the constitutive law in Glimm, Plohr, and Sharp [12]; the major difference is that the stress in (6.5) is zero when $\partial v/\partial x = 0$, whereas the stress in [12] is never zero.

Upon discretization, we obtain a linear tridiagonal system of equations for v. The solution for v found above is then substituted in the energy balance equation (2.16), giving a nonlinear equation in the unknown $\theta(\cdot,t_{n+1})$ only. We solve the resulting equation using Newton's method, yielding a tridiagonal system of equations. The extrapolation θ^E is used as an initial guess, and one step of the Newton iteration is performed. At this point, approximations for both v and θ on the $n+1$st time level have been produced. Using these approximations as the new extrapolations, the entire iteration process is repeated until the difference between successive iterates is sufficiently small.

The automatic mesh refinement is based on the requirement that there are sufficiently many spatial grid points to resolve the steep velocity gradient. To resolve the strain rate adequately, we designed a grid refinement strategy so that there are always three or four grid points across the region of steep gradient. Since the height of this steep "jump" in the dimensionless velocity is roughly 1, the width of the jump is approximately $(\partial v/\partial x)^{-1}$. Thus, we refine if

$$\Delta x \geq \left(4 \max_{x\in[0,1]}\left|\frac{\partial v}{\partial x}\right|\right)^{-1}. \tag{6.6}$$

Near the shear band, small subintervals are needed to improve accuracy, while away from the band the solution is smooth and only a coarse mesh is required. Therefore, we introduce a local mesh refinement in a specified number of subintervals centered around the jump in velocity. Thus, near $x = 0$ the mesh becomes quite refined as multiple refinement steps are taken, while far from $x = 0$ there is little or no mesh refinement.

To test whether the time steps are sufficiently small, we examine the following integral identity at the point where the temperature is a maximum:

$$\theta(\cdot, t_n) = \left[\theta(\cdot, t_{n-1})^{-(p/m-1)} - \lambda\left(\frac{p-m}{m}\right)\int_{t_{n-1}}^{t_n} \theta^{-p/m}\sigma^{1+1/m}d\tau\right]^{-1/(p/m-1)}$$

$$\equiv \psi_n(\theta, \sigma). \tag{6.7}$$

This identity can be derived for the true solution and is used as follows. Once an approximation to the true solution is found at time t_{n+1} solving the nonlinear equations on the nth time step, we evaluate ψ_n using the approximations. We then compute the error $|\psi_n - \theta|$ at the point x where the approximate strain rate and temperature are at their maxima ($x = 0$ in the computations described in this section). If the error is greater than some predefined tolerance, the time step is shortened and the current approximation is recomputed.

In the accompanying figures, we first show the behavior of the *regular* perturbation solution formulae (4.39) and (4.40) and the *uniform* or blowup solution formulae (5.15) and (5.16) in comparison with the solutions *computed* by the finite-difference method described. Since we are comparing with the asymptotics, here we take $\lambda = 0$, which corresponds to the absence of heat conduction. We expect singular solutions because there is no unloading. We also show that the strain rate undergoes, at its maximum in x, a rapid growth which is possibly finite-time blowup.

The first graphs (Figures 6.1–6.5) show the highlights of the computation with parameters $\epsilon = 0.01$, $\alpha_1 = 23640$, $m = 0.3$, and $t \in [0, 1.22]$. We used an initial time step of $\Delta t = .001$ and an initial mesh of 500 subintervals. In the interpretation of these plots, we implicitly assume that the finite-difference approximation is considerably more accurate than the asymptotic formulas. Although this has not been proved rigorously for this case, it is known in a slightly simpler situation that the numerical solutions will be accurate as long as the true (continuous) solution is reasonably smooth (see French and Garcia [11]).

Figures 6.1 and 6.2 provide a comparison among the computed, regular asymptotic, and uniform asymptotic solutions for the temperature and strain rate at $t = 0.12$. The figures show that both the regular and uniform expansions are good approximations to the true solution, at least for "short" times.

Figures 6.3 and 6.4 provide the same comparisons at $t = 1.096$. We see that, as expected, for larger times the regular perturbation does not track as well as the uniform one does. Though we have imposed the symmetry condition (2.25), we note in the immediate neighborhood of $x = 0$, the temperature gradient θ_x is large. (In fact, θ_x decreases quickly to zero over a few grid points.) It is this near-discontinuous peak in θ that has motivated some authors to idealize the shear band as an inhomogeneity in the heat flux [8].

Figure 6.5 shows a comparison of the accuracy of the regular and uniform asymptotic expansions for the temperature as time progresses. The error plotted is the maximum relative error in the asymptotic expansion, which for this run always occurred at $x = 0$. The figure provides more evidence of the improved accuracy of the

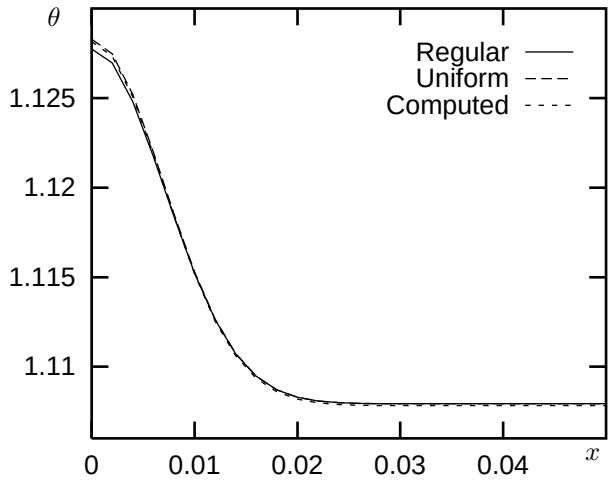

FIG. 6.1. *Comparison of computed, regular, and uniform approximations of* θ *vs.* x *for* $\epsilon = 0.01$, $\alpha_1 = 23640$, $\lambda = 0$, $m = 0.3$, *and* $t = 0.12$.

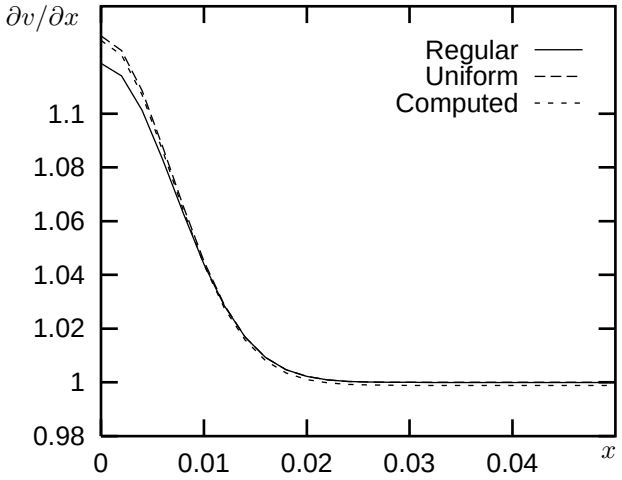

FIG. 6.2. *Comparison of computed, regular, and uniform approximations of* $\partial v/\partial x$ *vs.* x *for* $\epsilon = 0.01$, $\alpha_1 = 23640$, $\lambda = 0$, $m = 0.3$, *and* $t = 0.12$.

uniform expansion. However, once the strain rate begins to blow up, the uniform expansion starts to fail.

Figures 6.6–6.9 display the results of a computation that includes heat conduction and has $\alpha_1 = 2.364$, which corresponds to an extremely high characteristic strain rate. There may be some debate about the utility of the rigid/plastic approximation at such high strain rates. However, we follow the work of Wright and Walter, where they use the rigid/plastic approximation even at strain rates up to 5×10^4 s^{-1} [20], [24]. In Figure 6.6 we also include a plot that indicates the blowup behavior when $\lambda = 0$.

The initial amplitude of the perturbation is set to $\epsilon = 0.1$. In addition, we set $m = 0.3$ and $\lambda = 2.38 \times 10^{-5}$ in the heat conduction case. The mesh- and time-step refinement attributes of the numerical method are used to track the extreme

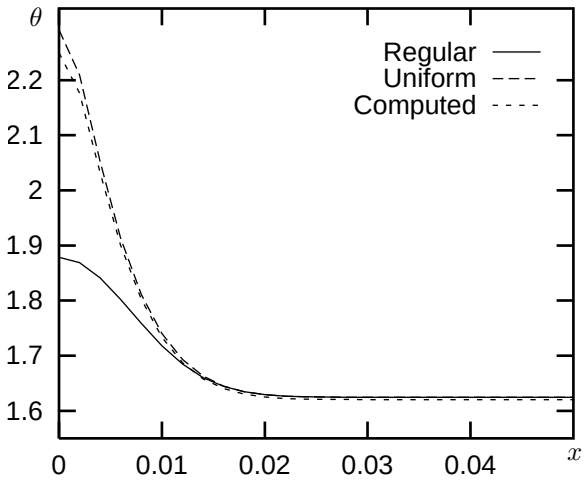

FIG. 6.3. *Comparison of computed, regular, and uniform approximations of θ vs. x for $\epsilon = 0.01$, $\alpha_1 = 23640$, $\lambda = 0$, $m = 0.3$, and $t = 1.096$.*

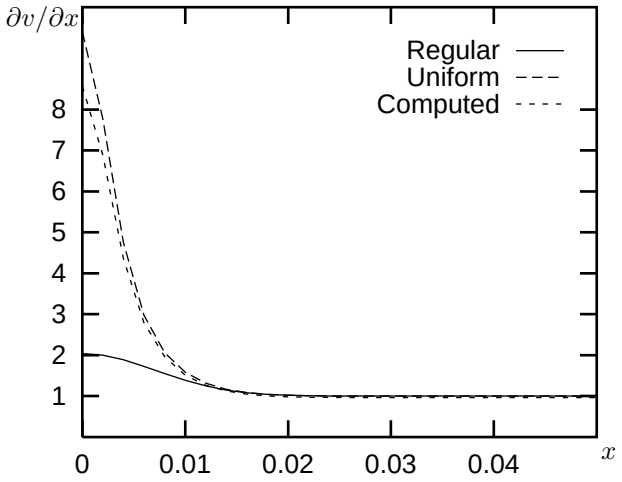

FIG. 6.4. *Comparison of computed, regular, and uniform approximations of $\partial v/\partial x$ vs. x for $\epsilon = 0.01$, $\alpha_1 = 23640$, $\lambda = 0$, $m = 0.3$, and $t = 1.096$.*

behavior of the strain rate and temperature. The mesh was refined many times once the severe localization process began. Initially, there were 250 subintervals, but when the computation stopped, there were 1510 intervals in the $\lambda = 0$ case and 628 intervals in the diffusion case. The time step was also reduced several times—initially it was 0.01, but when the computation stopped, it was 2×10^{-5} in the $\lambda = 0$ case and 2.5×10^{-3} in the diffusion case.

Figure 6.6 shows a plot of the maximum of the strain rate vs. t for the simplified model with $\lambda = 0$ and the full model with $\lambda \neq 0$. This plot provides strong evidence for finite-time blowup of the strain rate in the simplified model and that the simplified model is a good approximation of the more realistic model with diffusion. Also note that when heat conduction is included, not only does the strain rate not diverge, it

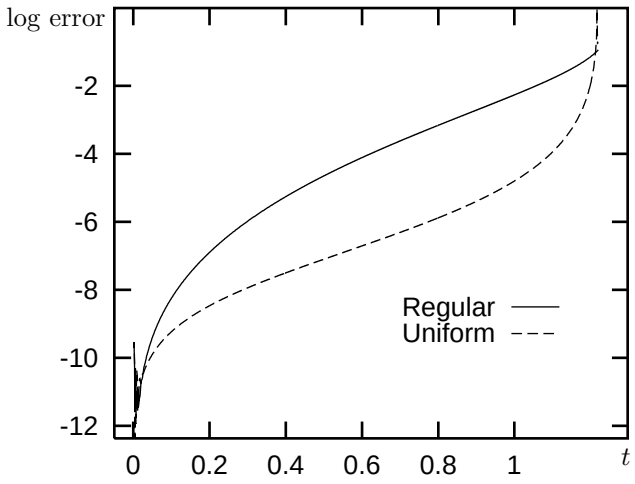

FIG. 6.5. *Comparison of the log of the relative errors in the approximation by the regular and uniform asymptotic expansions of θ vs. t for $\epsilon = 0.01$, $\lambda = 0$, $m = 0.3$, and $\alpha_1 = 23640$.*

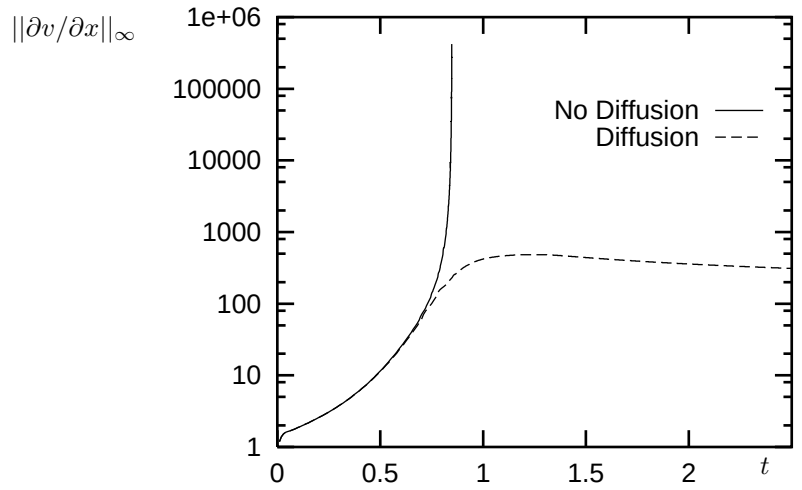

FIG. 6.6. *Computed strain rate maximums for cases with and without heat conduction (diffusion) plotted vs. time on a log/lin scale for $\epsilon = 0.1$ and $\alpha_1 = 2.364$.*

actually decreases after a certain period of time. This type of behavior is also seen in [4] and [13].

Figures 6.7–6.9 show the velocity, temperature, and stress functions plotted vs. x for the times shown in the diffusion case. In Figure 6.7 we see a shock structure forming for the velocity (the $t = 1.50$, $t = 2.00$, and $t = 2.50$ curves are on top of each other). At first, it evolves to a step function (the shock does widen slightly after the initial formation as in [13]). This is consistent with our physical understanding of the severe deformations associated with shear bands. Furthermore, Glimm, Plohr, and Sharp [12] have used a discontinuous velocity as an idealization of a shear band. We also note that this long-time step-function behavior is inconsistent with the outer solution (3.11). Therefore, our inner asymptotic expansions will certainly fail, since

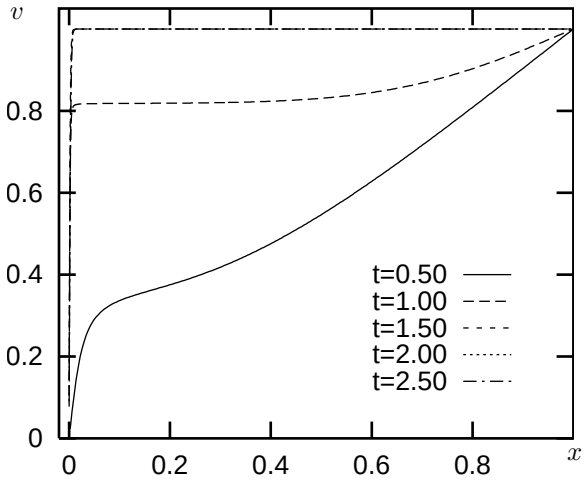

FIG. 6.7. *Computed v vs. x for $\epsilon = 0.1$, $\alpha_1 = 2.364$, $\lambda = 2.38 \times 10^{-5}$, and $t = 0.50$, 1.00, 1.50, 2.00, and 2.50.*

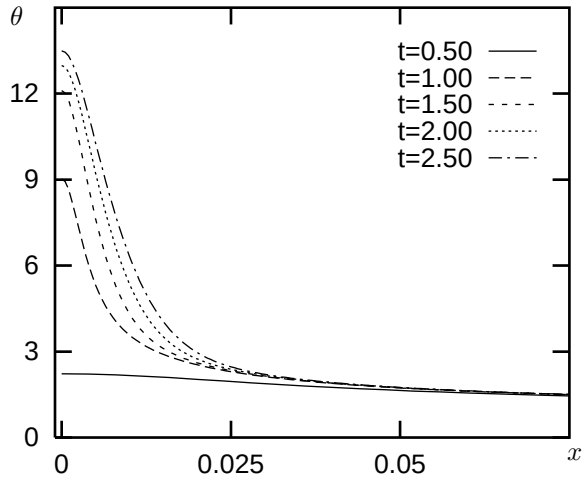

FIG. 6.8. *Computed θ vs. x for $\epsilon = 0.1$, $\alpha_1 = 2.364$, $\lambda = 2.38 \times 10^{-5}$, and $t = 0.50$, 1.00, 1.50, 2.00, and 2.50.*

they are matching to an incorrect solution as $\xi \to \infty$.

Figure 6.8 displays the growth of temperature in the center of the band as time progresses. The profiles are much smoother than in the previous case due to the presence of heat conduction, and they widen as a result of the same physical effect.

Figure 6.9 shows the stress weakening near the location of the imperfection. This weakening occurs only at very high strain rates [24]. We note that during this time interval and for this choice of α_1, the computed stress is not constant in the "outer" region away from the shear band. However, throughout our asymptotic analysis our solutions always had constant stress in the outer region to leading order. Therefore, we would expect that our asymptotic solutions would not be as accurate for small α_1, and this is indeed the case. (In fact, our leading-order asymptotic solutions do not

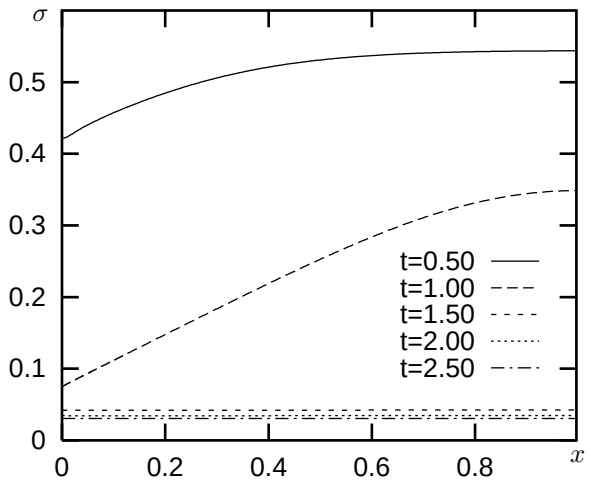

FIG. 6.9. *Computed* σ *vs.* x *for* $\epsilon = 0.1$, $\alpha_1 = 2.364$, $\lambda = 2.38 \times 10^{-5}$, *and* $t = 0.50$, 1.00, 1.50, 2.00, *and* 2.50.

even involve α_1.) The reason for this discrepancy can be found in (2.15). Figure 6.9 also shows that in the later stages of the computation the stress does become constant once the unloading stage begins.

We note that when considering the full equation, a large α_1 would force the stress to remain nearly constant regardless of the initial data. This is not the case for small α_1, and indeed when the strain rate is low, one sees nearly constant stress profiles [24].

7. Remarks on asymptotics with diffusion. To include the effects of diffusion, we redefine our parameter λ as $\lambda_0\epsilon^2$, where $\lambda_0 = O(1)$. Then the width of our perturbation given by (3.1) will indeed be of the correct diffusion scale. In this case, most of our analyses in sections 3–5 still hold, with the following exceptions.

Equation (2.16) becomes

$$\frac{\partial\theta}{\partial t} = \lambda_0\epsilon^2\frac{\partial^2\theta}{\partial x^2} + \alpha_2\sigma\frac{\partial v}{\partial x}, \tag{7.1}$$

which causes (4.3) to become

$$\frac{\partial\hat{\theta}}{\partial t} = \lambda_0\frac{\partial^2\hat{\theta}}{\partial\xi^2} + \frac{\alpha_2}{\epsilon}\hat{\sigma}\frac{\partial\hat{v}}{\partial\xi}. \tag{7.2}$$

Even though the dominant balance in (7.2) contains an additional term, since $z(t)$ depends only on time, the diffusion term vanishes and $z(t)$ satisfies (7.2). Therefore, our previous work in section 4 holds with (4.12) replaced by

$$\epsilon\frac{\partial\hat{\theta}_1}{\partial t} = \epsilon\left(\lambda_0\frac{\partial^2\hat{\theta}_1}{\partial\xi^2} + \alpha_2\sigma_0\frac{\partial\hat{v}_2}{\partial\xi} + \alpha_2 v_i\hat{\sigma}_1\right). \tag{7.3}$$

We again see that an initial layer is necessary. Equation (4.22) is replaced with

$$\epsilon^{-1}\frac{\partial\Theta}{\partial\eta} = \lambda_0\epsilon\frac{\partial^2\Theta}{\partial\xi^2} + \alpha_2\Sigma\left(v_i + \epsilon\frac{\partial V}{\partial\xi}\right), \tag{7.4}$$

which does not affect the analysis in that section either. However, upon returning back to our regular layer expansions, we see that by substituting our expression for $\hat{\sigma}_1$ into (7.3), we obtain the partial differential equation

$$\frac{1}{[g'(z)]^{1/m}}\frac{\partial \hat{\theta}_1}{\partial t} - \left\{\frac{1}{m}\frac{g''(z)}{[g'(z)]^{1/m+1}}\frac{dz}{dt}\right\}\hat{\theta}_1 = \frac{\lambda_0}{[g'(z)]^{1/m}}\frac{\partial^2 \hat{\theta}_1}{\partial \xi^2}, \tag{7.5}$$

which does not have the simple solution (4.34). However, we may solve (7.5) subject to our initial and boundary data (4.14) and (4.15). The solution is

$$\hat{\theta}_1(\xi,t) = \frac{g'(z)^{1/m}}{2\sqrt{\lambda_0 \pi t}}\int_0^\infty f'(\phi)\left\{\exp\left[-\frac{(\xi-\phi)^2}{4\lambda_0 t}\right] + \exp\left[-\frac{(\xi+\phi)^2}{4\lambda_0 t}\right]\right\} d\phi. \tag{7.6}$$

Our uniform solution is again given by our inner solution.

In the special case given by (3.17) and (4.38), the temperature given by

$$\theta(x,t) = z + \frac{\epsilon z^{p/m}}{\sqrt{4\lambda_0 t + 1}}\exp\left[-\frac{x^2}{\epsilon^2(4\lambda_0 t + 1)}\right]. \tag{7.7}$$

Note that (7.7) reduces to (4.39) in the limit that $\lambda_0 \to 0$.

There are several significant differences between (4.39) and (7.7). First, since diffusion now plays a role, our perturbation is smoothed out and becomes uniform in space as $t \to \infty$. This is consistent with the shear-band widening seen in DiLellio and Olmstead [7]. Due to the nature of the heat conduction operator, (7.7) has a term in it which decays like $t^{-1/2}$ for large time. However, since m is still small, we see that the solution resulting from our small perturbation still grows. Indeed, as before, the $O(\epsilon)$ term still grows faster than the $O(1)$ solution.

Replicating the analysis in section 5 while including the heat conduction term, we see that the analogue of (5.9) is

$$\frac{\partial \hat{\theta}_0}{\partial t} = \lambda_0 \frac{\partial^2 \hat{\theta}_0}{\partial \xi^2} + \frac{[g'(\hat{\theta}_0)]^{1/m}}{[g'(z)]^{1/m}}\frac{dz}{dt}. \tag{7.8}$$

The perturbation analysis of (7.8) is quite difficult and beyond the scope of this paper. However, we use some heuristic arguments to indicate that (7.8) will lead to bounded solutions.

As $\hat{\theta}_0$ grows larger and larger, so too will the stress term in (7.8), which is the second term on the right-hand side. As seen previously, in the absence of diffusion, this growth will occur in a narrow range. This growth in a narrow region will increase the size of the second-derivative term in (7.8), causing a dominant balance between the two terms on the right-hand side. Thus, the left-hand side of (7.8) may be neglected, consistent with the arguments in [12]. Since the stress term is always positive, we see that wherever we neglect the left-hand side of (7.8), the temperature is positive and concave down, which implies that there must be a maximum somewhere in that region.

8. Conclusions. The general model for shear bands presented in [4], [24], and elsewhere contains significant computational difficulties. However, simplified models hold the promise of obtaining qualitative agreement with experiments while being easier to solve. Therefore, we considered the case of a very high elastic shear modulus, which meant that the strain rate was equal to the velocity gradient. This rigid/plastic approximation has been used extensively (for instance, see [8], [12], [15], [20], and [24]).

In order to obtain asymptotic results, we began by neglecting heat conduction. Once a regular perturbation expansion was constructed for the case at hand, we saw that with the passage of time, the terms assumed to be small in the expansion came to dominate the "larger" terms. This caused the expansion to be suspect, and indeed when we compared the solutions constructed from the regular perturbation expansion to those calculated numerically, we saw that their validity was limited to very small times.

Since the regular perturbation expansion was of limited value, we next constructed a uniformly valid expansion by considering our perturbation to be of finite height. The resulting expression diverged at a finite time. Though the model without diffusion replicates the short-time evolution of the shear band well, the divergence of the solution is not physical. Since the model does not incorporate any way for the temperature profile to unload the heat generated by the plastic work term, the profile diverges, rather than spreading out as seen experimentally.

Even when the regularizing phenomenon of diffusion is included, the system is difficult to solve numerically. The shear band narrows severely and the strain rate becomes quite large on a short time scale. These phenomena require an algorithm with mesh- and time-step refinement capabilities. The numerical method we used appears to be effective at capturing the blowup behavior of the strain rate function in the model without diffusion. The numerical solutions show good agreement with the asymptotic ones.

Of course, once we include diffusion, the blowup is eliminated, as in [10]. The strain rate maximum at the center of the band peaks and then decays, as in [4]. We also note that the shear band begins to widen after a certain period, as in [7].

One can quite easily construct a regular perturbation expansion for the system with diffusion included. Since the second term in the expansion grows in an unacceptable manner, a uniformly valid approach is warranted. Though a complicated nonlinear partial differential equation results, through heuristic arguments it can be shown that the asympotic solution for the temperature (and hence the strain rate) will have maxima and hence remain bounded.

Though the model equations we have solved are simplified and do not capture the dynamics in all their generality, we were able to construct both asymptotic and numerical solutions which demonstrated good qualitative agreement with the physically observed phenomena. These results indicate that our methods hold great promise for more complicated models.

Appendix. Values of material parameters. With the laudable exceptions of [20] and [22], few papers in this field indicate the values of the actual physical parameters used to construct dimensionless parameters. We present a summary of some typical physical parameters below, as well as references where more detailed information may be found. Our motivation is threefold. First, we wish to run our numerical computations with reasonable values of our dimensionless parameters. Second, we wish to gain insight for how changes in the physical parameters would affect the mathematical formulation of our system. Last, we wish to see what changes in the physical parameters are plausible. For instance, a 1000-fold change in the strain rate is plausible, while a 1000-fold change in the yield stress is not.

Table A.1 indicates the values of several material parameters as tabulated in the listed references, as well as the value we used when calculating values of parameters for this paper.

For the characteristic strain rate $\dot{\gamma}_c$, we can use the nominal strain rate used for

TABLE A.1
Typical values of some material parameters. Calculated values are marked with asterisks.

Reference	k $\mathrm{kg \cdot m/(s^3 \cdot K)}$	κ 10^8 $\mathrm{kg/(m \cdot s^2)}$	ρ $\mathrm{kg/m^3}$	C_p $\mathrm{m^2/(s^2 \cdot K)}$	m
[17, Table 23-8]	48.46			502	
[17, Table 23-7]		6.3 (avg. *tensile*) 3.93 (avg. *yield*)	7750		
[20]	49.2	6.02	7860	473	0.0251
[21]	65				
[22]	46.7	5			
[23]		5	7800	500	0.022
[24]			6528*	544*	0.022
Used	53.5	5.08	7139	523	

the numerical calculations in Wright and Walter [24], which was 500 $\mathrm{s^{-1}}$. Wright [22] uses a strain rate of 1000 $\mathrm{s^{-1}}$. The maximal value of the strain rate used by Wright and Walter [24] was 50000 $\mathrm{s^{-1}}$. It is this value of the strain rate that led to sharp profiles and quick uptake times. We shall consider both extremes.

For a typical length scale, Wright [22] uses a value for d which doesn't reflect a true thickness. Glimm, Plohr, and Sharp [12], [13] and Walter [20] use a half-width of 3.47 mm, and it is this value which we shall use.

Wright [22] uses a characteristic temperature of $\theta_c = 300$ K. In Wright and Walter [24], the characteristic temperature can be computed from the other parameters in the paper, yielding $\theta_c = 164$ K. The small size of this characteristic temperature is not of concern since this has no direct relationship to the initial temperature distribution. Therefore, we use the value in Wright [22].

In order to calculate the elastic shear modulus μ, we begin by obtaining values of the regular elastic modulus. Perry and Green [17, Table 6-41] and the CRC [21, p. D-184] both give values of 2×10^{11} $\mathrm{kg/(m \cdot s^2)}$. Using the rule of thumb given in Kutz [14], which says that the shear modulus is usually about 0.4, the elastic modulus for metals, we obtain $\mu = 8 \times 10^{10}$ $\mathrm{kg/(m \cdot s^2)}$. The same value is also given in Batra [2], Smith [18, pp. 19–20], and Walter [20].

Using the parameters noted above, we see that the parameter in the stress evolution equation is given by $\kappa/\mu = 6.25 \times 10^{-3}$. Since this quantity is quite small, it is reasonable to take it equal to zero, as we did in section 2. In addition, λ is given by

$$2.38 \times 10^{-5} \leq \lambda \leq 2.38 \times 10^{-3}, \tag{A.1}$$

depending on the value of the strain rate we use.

We see that α_1 is in the range given by

$$2.364 \leq \alpha_1 \leq 2.364 \times 10^4, \tag{A.2}$$

depending on the value of the strain rate we use. If we use the largest strain rate in [24], we obtain the lower bound. However, if we use more physically attainable strain rates, α_1 approaches the upper bound. Therefore, we see that our analysis in section 6 holds. With our chosen parameters, we have $\alpha_2 = 0.454$, and this term must be retained in the analysis.

Nomenclature.

Variables and parameters. Units are listed in terms of length (L), mass (M), time (T), or temperature (Θ). If the same letter appears both with and without a tilde, the letter with a tilde has dimensions, while the letter without a tilde is dimensionless. If the same letter appears in boldface and italics, the boldface letter is a vector of which the italic letter is a component. The equation where a quantity first appears is listed, if appropriate.

$\mathcal{C}$: 4-tensor of elastic moduli, units M/T^2L (2.3).
C_p: heat capacity at constant pressure per unit mass, units $L^2/T^2\Theta$ (2.2).
D: diffusion coefficient in short-time equation, value $\alpha_1 m v_i^{m-1}$ (4.30).
d: double-precision roundoff error (6.5).
$f(\cdot)$: function characterizing the perturbation in the temperature (3.2).
$\tilde{g}'(\tilde{\theta})$: stress-hardening function, units T^{-m} (2.7).
H: thickness of the solid, units L.
$h(\xi,\eta)$: displacement variable in short-time evolution equation (4.29).
k: thermal conductivity, units $ML/T^3\Theta$ (2.2).
m: exponent in Ostwald-de Waele stress-strain model (2.7).
n: indexing variable (6.3).
p: exponent in stress-hardening model (3.17).
$\tilde{t}$: dimensional time, units T (2.1).
$U(\theta)$: integral quantity used in numerical scheme (6.2).
$V(\xi,\eta)$: short-time solution for velocity (4.19).
$\tilde{\mathbf{v}}$: velocity, units L/T (2.1).
w: velocity derivative (5.3).
$\tilde{x}$: dimensional measure of length along the sample, units L (2.4).
$\tilde{y}$: dimensional measure of length in the direction of shear, units L (2.4).
$\mathcal{Z}$: the integers.
z: leading-order outer solution for temperature; also treated as an independent variable (3.3).
α: coefficient in dimensionless system (2.18).
β: dimensionless parameter, value $(p+1)\alpha_2 v_i^{m+1}$ (3.18).
$\dot{\tilde{\Gamma}}_p$: rate of plastic strain tensor, units T^{-1} (2.2).
$\dot{\gamma}$: rate of plastic strain (2.12).
δ: dimensionless parameter used to represent larger perturbations, usually taken to be $\epsilon f'(\xi)$ (5.2).
ϵ: small dimensionless parameter characterizing the spatial inhomogeneity of the perturbation, also used in perturbation expansions (3.2).
η: short-time variable, defined as $t\epsilon^{-2}$ (4.19).
$\Theta(\xi,\eta)$: short-time solution for velocity (4.19).
$\tilde{\theta}$: temperature, units Θ (2.2).
κ: stress-hardening coefficient, units M/T^2L (2.7).
λ: coefficient of thermal diffusion term in dimensionless heat equation (2.18).
μ: elastic shear modulus, units M/T^2L (2.6).
ξ: boundary-layer variable, defined as $x\epsilon^{-1}$ (4.1).
ρ: density, units M/L^3 (2.1).
$\Sigma(\xi,\eta)$: dimensionless stress in short-time region (4.19).
σ: dimensionless stress (2.13).
$\tilde{\tau}$: stress tensor, units M/T^2L (2.1).
ϕ: dummy variable, variously defined (4.32).

ψ: expression in integral identity (6.7) used in numerical method.

Other notation.

b: as a subscript, used to indicate the curve $\delta(z)$ along which the solution blows up.

c: as a subscript, used to indicate the characteristic value of a quantity (2.12).

E: as a superscript, used to indicate an extrapolated quantity (6.3).

i: as a subscript, used to indicate the initial state of a quantity (2.9).

$j \in \mathcal{Z}$: as a subscript, used to itemize α (2.16), to indicate a term in an expansion (3.3), or to index time (6.3).

p: as a subscript, used to indicate the plastic strain rate (2.2).

$\tilde{x}$: as a subscript, used to indicate a component in the $\tilde{x}$ direction (2.4).

$\tilde{y}$: as a subscript, used to indicate a component in the $\tilde{y}$ direction (2.4).

$\hat{}$: used to denote a variable in the boundary layer (4.1).

Acknowledgments. The authors wish to thank Reza Malek-Madani, Dawn A. Lott-Crumpler, and W. Edward Olmstead for helpful discussions of the problem and the reviewers for their insightful comments which improved the manuscript. Many of the calculations herein were checked with Maple.

REFERENCES

[1] Y. Bai and B. Dodd, *Adiabatic Shear Localization: Occurrence, Theories and Applications*, Pergamon Press, Oxford, 1992.

[2] R. C. Batra, *Effect of material parameters on the initiation and growth of adiabatic shear bands*, Internat. J. Solids Structures, 23 (1987), pp. 1435–1446.

[3] R. C. Batra and K. I. Ko, *An adaptive mesh refinement technique for the analysis of shear bands in plane strain compression of a thermoviscoplastic solid*, Comput. Mech., 10 (1992), pp. 369–379.

[4] A. Bayliss, T. Belytshko, M. Kulkarni, and D. A. Lott-Crumpler, *On the dynamics and the role of imperfections for localization in thermo-viscoelastic materials*, Mod. Sim. Mat. Sci., 2 (1994), pp. 941–964.

[5] R. B. Bird, W. E. Stewart, and E. N. Lightfoot, *Transport Phenomena*, John Wiley, New York, 1960.

[6] G. F. Carrier and C. E. Pearson, *Partial Differential Equations: Theory and Technique*, 2nd ed., Academic Press, Boston, 1988.

[7] J. A. DiLellio and W. E. Olmstead, *Temporal evolution of shear band thickness*, J. Mech. Phys. Solids, 45 (1997), pp. 345–359.

[8] J. A. DiLellio and W. E. Olmstead, *Shear band formation due to a thermal flux inhomogeneity*, SIAM J. Appl. Math., 57 (1997), pp. 959–971.

[9] D. A. Drew and J. E. Flaherty, *Adaptive finite element methods and the numerical solution of shear band problems*, in Phase Transformations and Material Instabilities in Solids, Academic Press, Orlando, 1984, pp. 37–60.

[10] D. A. French, *Computation of large shear deformations of a thermoplastic material*, Numer. Methods Partial Differential Equations, 12 (1996), pp. 393–406.

[11] D. A. French and S. M. F. Garcia, *Finite element approximation of an evolution problem modeling shear band formation*, Comput. Methods Appl. Mech. Engrg., 118 (1994), pp. 153–163.

[12] J. G. Glimm, B. J. Plohr, and D. H. Sharp, *A conservative formulation for large-deformation plasticity*, Appl. Mech. Rev., 46 (1993), pp. 519–526.

[13] J. G. Glimm, B. J. Plohr, and D. H. Sharp, *Tracking of shear bands* I: *The one-dimensional case*, Mech. Mat., 24 (1996), pp. 31–41.

[14] M. Kutz, ed., *Mechanical Engineers' Handbook*, John Wiley, New York, 1986.

[15] J. H. Maddocks and R. Malek-Madani, *Steady-state shear bands in thermoplasticity*—I: *Vanishing yield stress*, Internat. J. Solids Structures, 29 (1992), pp. 2039–2061.

[16] A. Needleman, *Dynamic shear band development in plane strain*, J. Appl. Mech., 56 (1989), pp. 1–9.

[17] R. H. Perry and D. W. Green, eds., *Perry's Chemical Engineers' Handbook*, 6th ed., McGraw-Hill, New York, 1984.
[18] E. H. Smith, ed., *Mechanical Engineer's Reference Book*, 12th ed., Butterworth-Heinemann, Oxford, 1994.
[19] A. E. Tzavaras, *Effect of thermal softening in shearing of strain-rate dependent materials*, Arch. Rational Mech. Anal., 99 (1987), pp. 349–374.
[20] J. W. Walter, *Numerical experiments on adiabatic shear band formation in one dimension*, Internat. J. Plast., 8 (1992), pp. 657–693.
[21] R. C. Weast, ed., *CRC Handbook of Chemistry and Physics*, 68th ed, CRC Press, Boca Raton, 1987.
[22] T. W. Wright, *Steady shearing in a viscoplastic solid*, J. Mech. Phys. Solids, 35 (1987), pp. 269–282.
[23] T. W. Wright, *Approximate analysis for the formation of adiabatic shear bands*, J. Mech. Phys. Solids, 38 (1990), pp. 515–530.
[24] T. W. Wright and J. W. Walter, *On stress collapse in adiabatic shear bands*, J. Mech. Phys. Solids, 35 (1987), pp. 701–720.